Int. J. Electrochem. Sci., 17 **(2022)** Article Number: 2212105, doi: 10.20964/2022.12.96

International Journal of
ELECTROCHEMICAL
SCIENCE
www.electrochemsci.org

Short Communication

Highly Sensitive Detection of miRNA-21 Based on Electrochemical Immunosensor

Yue Shi[1], *Qi Wang*[2] *and Fengqin Xu*[3,4,*]

[1] Graduate School, Beijing University of Chinese Medicine, Chaoyang, Beijing, 100029, China
[2] Jilin Institute of Applied Chemistry, Changchun 130022, China
[3] Xiyuan Hospital, China Academy of Chinese Medical Sciences, Haidian, Beijing, 100091, China
[4] Institute of Geriatrics, China Academy of Chinese Medical Sciences, Haidian Beijing, 100091, China
[*]E-mail: fengqinxu_edu@163.com

Received: 26 October 2022 / *Accepted:* 10 December 2022 / *Published:* 27 December 2022

Inflammation is one of the main mechanisms of neurological damage after ischemia and hypoxia in brain tissue and plays an important role in the progression of ischemic stroke. Microglia, as intrinsic immune cells of the central nervous system, are involved in the pathophysiological process of cerebral ischemia by mediating inflammation. miRNA-21 may be involved in the pathophysiology of diseases such as ischemic stroke and atherosclerosis through the regulation of inflammatory processes. In this work, methylene blue-modified stem-loop structural probes were immobilized on the sensor surface. With the addition of miRNA-21, the signal of methylene blue is gradually diminished. Therefore, the quantitative detection of miRNA-21 can be achieved by the alteration of electrochemical signal.

Keywords: Stroke; Aptamer sensor; Methylene blue; Electrochemical properties; Cardiovascular

1. INTRODUCTION

Stroke is a common clinical disease of the elderly with a high mortality rate, and survivors also tend to have symptoms of neurological deficits such as aphasia and hemiparesis. Cerebral ischemic stroke is the most prevalent and harmful of all stroke types, and effective ischemia-reperfusion therapy is often limited by the time window for treatment as well as hospital care conditions[1,2]. Continuous ischemia and hypoxia cause irreversible damage to brain tissue, and inflammation is one of the main mechanisms of post-ischemic neurological injury [3,4]. Microglia, as intrinsic immune cells of the central nervous system, are involved in the pathophysiological process of cerebral ischemia by mediating inflammation [5–7]. miRNAs are a class of endogenous non-coding small RNAs that regulate gene expression at the post-transcriptional level by degrading target miRNAs or inhibiting their translation-negative properties [8].

miRNAs are a class of small endogenous non-coding RNAs of approximately 22nt in length that are highly conserved. miRNAs play an important role in biological processes such as inflammation, apoptosis, development, proliferation, differentiation, and angiogenesis [9,10]. It has been shown that 30-90% of human genes are regulated by miRNAs. Microglia are mesodermal-derived myeloid cells that arise during the primitive hematopoiesis of the yolk sac and have potent chemotactic, phagocytic, antigen-presenting, and cytokine secreting abilities [11]. The human cerebral cortex is composed of 20-25 billion neurons, of which microglia account for 6-18% of the cells in the cerebral cortex. miRNAs, as important regulators of biological functions, are involved in microglia development, differentiation and activation [12,13]. Among them, miRNA-21 may be involved in the pathophysiological processes of diseases such as ischemic stroke and atherosclerosis by regulating inflammatory processes. Therefore, there is a need to establish detection technology for miRNA-21[14].

The traditional methods for detecting miRNAs include three main types: northern analysis, microarray analysis and quantitative real-time polymerase chain reaction (qRT-PCR) [15–20]. Among them, qRT-PCR has become the most commonly used method in clinical testing. Compared to the other two techniques, it has the advantages of high sensitivity and low sample usage. However, the extraction, amplification and calibration steps are time-consuming, and the amplification may affect the accuracy of the experiment [21–23]. Therefore, there is a need to design some rapid, sensitive and economical assays to enable the analysis of miRNAs to an idealized level.

Aptamer refers to a class of single-stranded oligonucleotide fragments that can specifically bind to target molecules. Aptamer, due to its high affinity and specificity with ligands, aptamers can be widely used in analytical studies in biological and environmental fields [24–27]. Electrochemical analysis is a fast, economical and sensitive method. It greatly increases the sensitivity of the method by direct or indirect labeling in combination with signal amplification strategies [28–30]. In this work, we immobilized the methylene blue modified stem-loop structure probe on the surface of the gold electrode through a gold-sulfur bond. The presence of the stem-loop structure will make methylene blue close to the electrode surface and detect a strong electrochemical signal. With the addition of miRNA-21, miRNA-21 hybridizes with the probe via base complementary pairing resulting in stem-loop opening. This process moves the methylene blue away from the electrode surface, causing a decrease in the electrochemical signal. Therefore, the quantitative detection of miRNA-21 can be achieved by the alteration of the electrochemical signal.

2. EXPERIMENTAL

2.1. Chemicals

Tris(hydroxymethyl) aminomethane (Tris), Tris(2-Carboxyehtyl) phosphine hydrochloride (TCEP), 6-mercaptohexanol (MCH), potassium ferricyanide ($K_3[Fe(CN)_6]$), potassium ferricyanide trihydrate ($K_4[Fe(CN)_6]$-$3H_2O$), methylene blue (MB), disodium hydrogen phosphate (Na_2HPO_4), potassium dihydrogen phosphate (KH_2PO_4), and sodium perchlorate ($NaClO_4$) were purchased from Sinopharm Chemical Reagent Co. Chloroauric acid ($HAuCl_4$-$3H_2O$) was purchased from Sigma, and the

solvent for all solutions during the experiments was ultrapure water, prepared by a Milli-Q water purifier (Milliproe Ltd.) with a resistivity of 18 MΩ·cm. The probes and miRNA-21 were purchased from Shanghai Bioengineering Co. The sequences of the DNA synthesized are listed in the following table 1.

Table 1. Sequence of the DNA used for the experiment.

	Sequence (5'-3')
A1	5'-GCGAGGTATCAACATCAGTCTGATAAGCTACCTCGC–$(CH_2)_6$-SH-3'
A2	5'-MB-GCGAGGTATCAACATCAGTCTGATAAGCTACCTCGC-$(CH_2)_6$-SH-3'
miRNA-21	UAGCUUAUCAGACUGAUGUUGA

2.2. Sensor fabrication

All electrochemical assays were performed on an electrochemical workstation (CHI760E) with a conventional three-electrode system: Au electrode as the working electrode, platinum wire counter electrode as the counter electrode, and Ag/AgCl electrode as the reference electrode. The gold electrode was first soaked in Piranha solution for 30 min, and rinsed with water. Then, the gold electrode was polished with 1 μm, 0.3 μm and 0.05 μm alumina powder on the flannel surface until the gold electrode was mirror-like without scratches, and sonicated in ultrapure water and anhydrous ethanol for 5 min each. Finally, the electrode surface was rinsed with ultrapure water and blown dry with nitrogen gas.

1 μM A2 was mixed with 10 mM TCEP and fixed to 200 μL with Tris-HCl buffer and placed in the dark for 1 h to reduce the disulfide bonds. After the reaction, the pretreated electrode was immersed in the above A2 solution and incubated overnight at room temperature in the dark, followed by sufficient washing with 0.1 M PBS buffer and ultrapure water to remove the non-specific adsorbed A2 (denoted as A2/Au). Finally, the electrode was incubated with 2 mM MCH for 2 h to obtain the monolayer self-assembled structure of A2 on the surface of the Au electrode (denoted as MCH/A2/Au).

2.3. miRNA-21 detection

The modified electrodes were mixed with different concentrations of miRNA-21 solution and incubated for 2 h (denoted as MCH/A2/Au(miRNA-21)). After the reaction, alternating current voltammetry (ACV) scan were performed using a three-electrode system. After each step, the modified electrodes were washed with 0.1 M PBS buffer in order to clean off the various molecules physically adsorbed on the electrode surface. EIS tests were performed at frequencies ranging from 0.1 Hz to 10 kHz with an alternating voltage of 5 mV. all tests were performed in a solution containing 5.0 mM $[Fe(CN)_6^{3-/4-}]$.

3. RESULTS AND DISCUSSION

A2 is immobilized on the surface of the gold electrode through a gold-sulfur bond. The presence of the stem ring structure will make the MB close to the electrode surface, where electron transfer occurs and a strong electrochemical signal is detected. With the addition of miRNA-21, miRNA-21 hybridizes with A2 by base-complementary pairing and leads to stem-loop opening [31,32]. This causes the MB to move away from the electrode surface, impeding the electron transfer between them, and the electrochemical signal is reduced. The reduction value of electrochemical signal was proportional to the amount of miRNA-21 incorporation within a certain range [33]. Based on this, an electrochemical biosensor based on the stem-loop structure can be constructed for the quantitative detection of miRNA-21.

EIS was used to characterize the modification process of the electrode. Figure 1 represents Nyquist plots of the EIS measured in 5.0 mM $[Fe(CN)_6^{3-/4-}]$ solution and fitted by Randles. In the figure, it can be seen that the bare Au electrode presents a very small semicircle, which indicates a good electron transfer on the surface of the Au electrode [34]. When A2 is assembled by gold-sulfur bonding, the semicircle diameter increases because A2 has a negatively charged phosphate backbone. When it is fixed on the electrode surface, it will hinder the electron transfer between $[Fe(CN)_6^{3-/4-}]$ and the electrode by electrostatic repulsion. After MCH confinement, the impedance value increases further, which is due to the fact that MCH itself is non-conductive. When immobilized on the electrode surface it is able to remove non-specific adsorbed A2, reducing the accessibility of the electrochemical probe and hindering electron transfer [35]. When miRNA-21 was added, the impedance value was said to increase relative to the MCH closure. This suggests that the specific binding of miRNA-21 to A2 increases the negative charge density of the phosphate backbone, further impeding the electron transfer at the interface between the redox probe and the electrode.

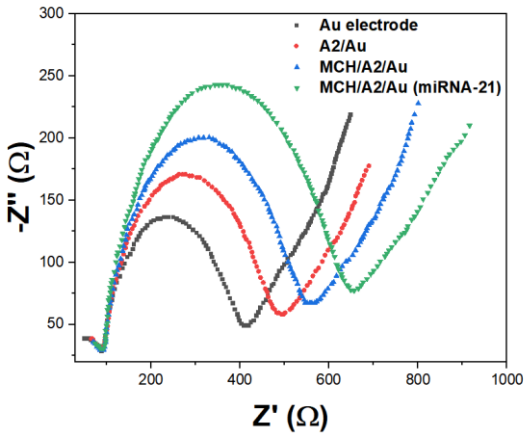

Figure 1. EIS of bare Au, A2/Au, MCH/A2/Au and MCH/A2/Au(miRNA-21) in 5.0 mM $[Fe(CN)_6^{3/4-}]$.

To further demonstrate the feasibility of this chemical sensor, we chose ACV to detect the electrochemical signal of the electrode assembly process. The results are shown in Figure 2. The

electrode was first modified with hairpin A2 and MCH, and the measured current value of ACV signal was small [36]. When the electrode further interacted with the target miRNA-21 and hairpin H2, the signal value increased somewhat. This indicates that our constructed electrochemical sensor can amplify the signal [37]. This result further indicates that our constructed electrochemical sensor can detect the target material sensitively and achieve signal amplification [38].

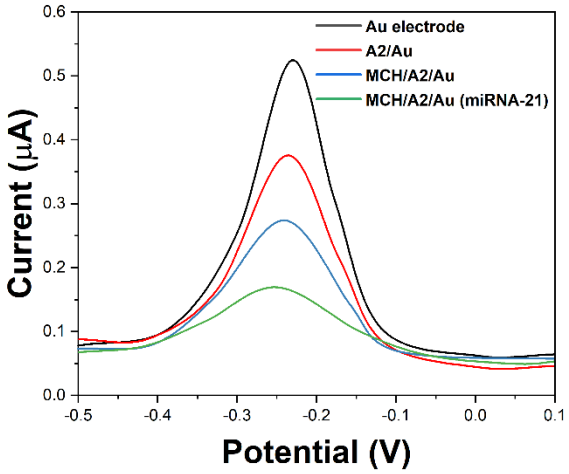

Figure 2. ACV responses of bare Au, A2/Au, MCH/A2/Au and MCH/A2/Au(miRNA-21) in 5.0 mM $[Fe(CN)_6^{3/4-}]$.

In order to improve the conductivity of the sensor, a series of experimental conditions were optimized, including the concentration of the hairpin A2 fixed on the surface of the gold electrode, and the incubation time of the electrode with the hairpin A2 [39]. The concentration of hairpin A2 modified on the surface of the gold electrode had a large influence on the experimental system. We chose the concentrations of 0.1 μM, 0.3 μM, 0.5 μM, 0.7 μM, and 0.9 μM. It can be seen from Figure 3A that the electrochemical signal started to enhance significantly with the increase of hairpin A2 concentration. However, the current signal reached the maximum when the DNA concentration reached 0.5 μM. After that the current signal decreases instead with the increase of the concentration. This may be due to the fact that as the concentration of hairpin A2 increases, the density of hairpins modified on the surface of the gold electrode increases, further increasing the spatial potential resistance [40]. Figure 3B shows the optimization of the incubation time for the modified electrodes with the target and hairpin A2. It can be seen that the current signal is increasing with the increase of the reaction time. After the reaction time reaches 90 min, the current signal difference no longer increases as the reaction time increases, so we choose the optimal incubation time of 90 min.

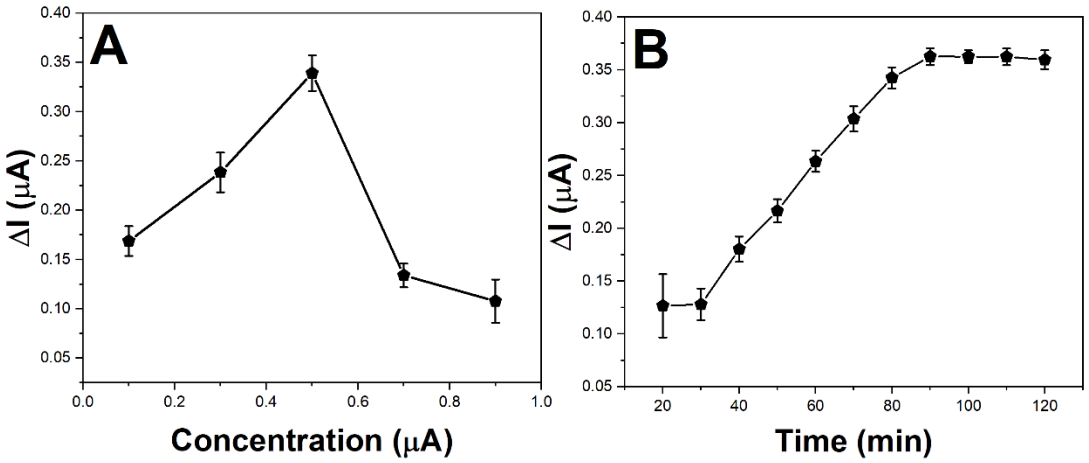

Figure 3. (A) Optimization of A2 concentration immobilized on the gold electrode. (B) Optimization the time of electrode incubated with miRNA-21 and A2.

In order to investigate the sensitivity of the sensor, the electrochemical response signal of the sensor to different concentrations of miRNA-21 was measured in this experiment, and the experimental results are shown in Figure 4. Figure 4A reflects the ACV spectra of this sensor obtained with the addition of different concentrations of miRNA-21. It can be seen from the figure that the electrochemical signal of this sensing system gradually decreases as the concentration of miRNA-21 increases from 0 to 10 μM. Figure 4B shows the calibration curve of this electrochemical sensor. The logarithm of the percentage reduction of the electrochemical signal and miRNA-21 concentration showed a good linearity in the range of 10 fM-100 nM with the correlation coefficient R^2= 0.9884. The detection limit of the method can be calculated as 3.2 fM by equation 3 σ/s. Table 2 shows the sensing performance comparison of proposed sensor with previous reports.

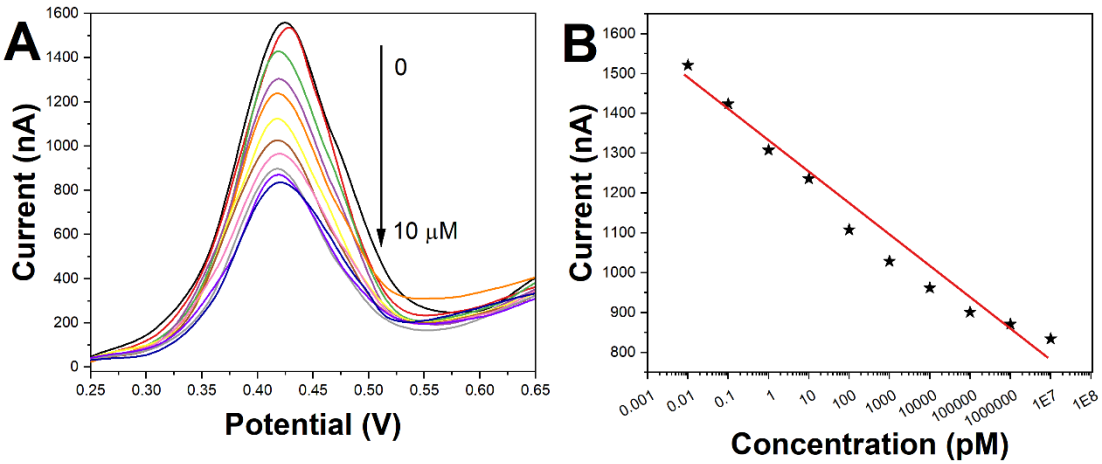

Figure 4. (A) ACV response of the MCH/A2/Au after the addition of various concentrations of miRNA-21 (0, 10 fM, 100 fM, 1 pM, 10 pM, 100 pM, 1 nM, 10 nM, 100 nM, 1 μM, 10 μM) in 5.0 mM [$Fe(CN)_6^{3/4-}$]. (B) The signal decease (%) of the aptasensor as a function of miRNA-21 concentration. Inset: calibration curve for log miRNA-21.

Table 1. Sensing performance of the proposed MCH/A2/Au with previous reports towards miRNA-21 detection.

Sensor	Linear range	LOD	Ref.
DNA modified gold electrode using iridium(III) complex as catalyst	5 fM-1 pM	1.6 fM	[41]
DNA modified gold electrode with DSN-assisted target recycling	0.05 fM-5 fM	0.01 fM	[42]
MB on ss-DNA and miRNA/DNA	0.1 to 500.0 pM	84.3 fM	[43]
MCH/A2/Au	10 fM-100 nM	3.2 fM	This work

The response signals of 0.1 nM miRNA-21, single-base mismatch miRNA, tri-base mismatch miRNA, and fully non-complementary miRNA were detected by this sensor. As shown in Figure 5, the detection signals of single-base mismatch miRNA, tri-base mismatch miRNA and fully non-complementary miRNA were weak, 12.8%, 7.1% and 6.9% of the detection signal of miRNA-21, respectively, indicating that the sensor has good specificity.

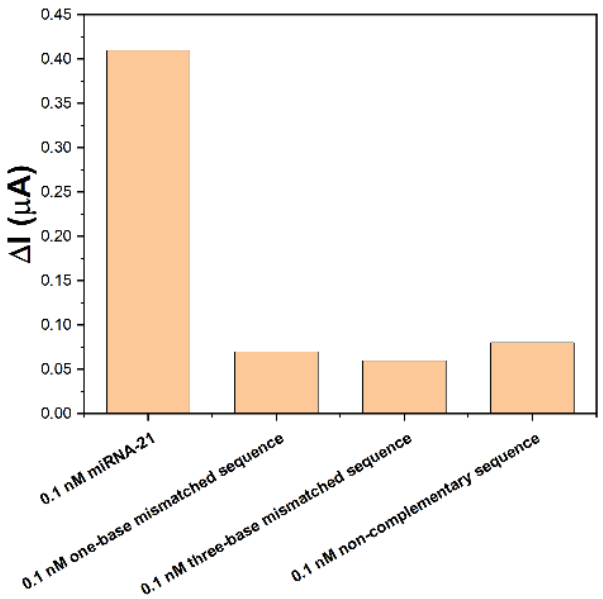

Figure 5. Specificity test of the proposed aptamer sensor towards 0.1 nM miRNA-21, 0.1 nM one-base mismatched sequence, 0.1 nM three-base mismatched sequence and 0.1 nM non-complementary sequence.

The usefulness of the sensor was examined by measuring miRNA-21 in whole blood and serum samples from mice. No miRNA-21 was detected in mouse whole blood and serum. the results of the

standard spiked experiments are shown in Table 3 and Table 4. The results showed that the spiked recoveries in mouse serum ranged from 93.2% to 107.8%, and the RSD was less than 5.1%. The spiked recoveries in whole blood lysate ranged from 98.5% to 108.9%, with RSD less than 6.6%. The results showed that the sensor is practical and can be used for the detection of real samples [44].

Table 3. Detection results of miRNA-21 in mouse serum sample using MCH/A2/GCE.

No.	Added (pM)	Found (pM)	RSD (%)	Recovery (%)
1	1.00	0.93	3.7	93.2
2	10.00	9.45	5.1	94.5
3	100.00	107.00	5.1	107.0
4	1000.00	992.00	3.6	99.2
5	10000.00	10780.00	2.5	107.8

Table 4. Detection results of miRNA-21 in diluted mouse whole blood using MCH/A2/GCE.

No.	Dilution	Added (pM)	Found (pM)	RSD (%)	Recovery (%)
1	Diluted by 1000 times	-	166	4.2	-
2	Diluted by 500 times	-	305	6.6	-
3	Diluted by 500 times	100	441	2.7	108.9
4	Diluted by 500 times	300	621	3.3	102.6
5	Diluted by 500 times	1000	1285	2.9	98.5

4. CONCLUSION

This work constructed an electrochemical biosensor for miRNA-21 detection. In the concentration range of miRNA-21 from 10 fM to 100 nM, the sensor showed a good linear relationship between the percentage reduction of electrochemical signal and the logarithmic value of miRNA-21 concentration, and this experiment has the advantages of simple operation, low cost and less time consuming compared with the traditional detection means.

References

1. M. Kawabori, H. Shichinohe, S. Kuroda, K. Houkin, *International Journal of Molecular Sciences*, 21 (2020) 7380.
2. X. Wang, W. Xuan, Z. Zhu, Y. Li, H. Zhu, L. Zhu, D. Fu, L. Yang, P. Li, W. Yu, *CNS Neuroscience & Therapeutics*, 24 (2018) 1100–1114.
3. J. Yang, M. Chen, R.Y. Cao, Q. Li, F. Zhu, *Circular RNAs* (2018) 309–325.

4. R. Chen, Y. Xu, P. Wu, H. Zhou, Y. Lasanajak, Y. Fang, L. Tang, L. Ye, X. Li, Z. Cai, *Pharmacological Research*, 148 (2019) 104403.
5. Y. Zheng, R. He, P. Wang, Y. Shi, L. Zhao, J. Liang, *Biomaterials Science*, 7 (2019) 2037–2049.
6. A. Otxoa-de-Amezaga, F. Miró-Mur, J. Pedragosa, M. Gallizioli, C. Justicia, N. Gaja-Capdevila, F. Ruíz-Jaen, A. Salas-Perdomo, A. Bosch, M. Calvo, *Acta Neuropathologica*, 137 (2019) 321–341.
7. X. Tian, H. Liu, F. Xiang, L. Xu, Z. Dong, *Life Sciences*, 237 (2019) 116915.
8. M. Giordano, M.C. Trotta, T. Ciarambino, M. D'Amico, M. Galdiero, F. Schettini, D. Paternosto, M. Salzillo, R. Alfano, V. Andreone, *International Journal of Molecular Sciences*, 21 (2020) 7615.
9. T. Forró, Z. Bajkó, A. Bălașa, R. Bălașa, *International Journal of Molecular Sciences*, 22 (2021) 5621.
10. A. Gugliandolo, S. Silvestro, C. Sindona, P. Bramanti, E. Mazzon, *Medicina*, 57 (2021) 1053.
11. C. Eyileten, Z. Wicik, S. De Rosa, D. Mirowska-Guzel, A. Soplinska, C. Indolfi, I. Jastrzebska-Kurkowska, A. Czlonkowska, M. Postula, *Cells*, 7 (2018) 249.
12. Y. Qian, M. Chopp, J. Chen, *Experimental Neurology*, 331 (2020) 113382.
13. M. Qu, J. Pan, L. Wang, P. Zhou, Y. Song, S. Wang, L. Jiang, J. Geng, Z. Zhang, Y. Wang, *Molecular Therapy-Nucleic Acids*, 16 (2019) 15–25.
14. E. Jayawardena, L. Medzikovic, G. Ruffenach, M. Eghbali, *International Journal of Molecular Sciences*, 23 (2022) 1512.
15. J. Li, R. Cai, W. Tan, *Anal. Chem.*, 94 (2022) 12280–12285.
16. T. Yao, L. Kong, Y. Liu, H. Li, R. Yuan, Y. Chai, *Anal. Chem.*, 94 (2022) 12256–12262.
17. J. Parchekani, H. Hashemzadeh, A. Allahverdi, H. Siampour, S. Abbasian, A. Moshaii, H. Naderi-Manesh, *Sensing and Bio-Sensing Research*, 34 (2021) 100449.
18. L. Gutiérrez-Gálvez, T. García-Mendiola, C. Gutiérrez-Sánchez, T. Guerrero-Esteban, C. García-Diego, I. Buendía, M.L. García-Bermejo, F. Pariente, E. Lorenzo, *Microchimica Acta*, 188 (2021) 398.
19. C.-H. Huang, T.-T. Huang, C.-H. Chiang, W.-T. Huang, Y.-T. Lin, *Biosensors and Bioelectronics*, 164 (2020) 112320.
20. H.F. Hetta, A.M. Zahran, E.A. Shafik, R.I. El-Mahdy, N.A. Mohamed, E.E. Nabil, H.M. Esmaeel, O.A. Alkady, A. Elkady, D.A. Mohareb, *Microrna*, 8 (2019) 206–215.
21. M. Selvaraj, P. Greco, M. Sensi, G.D. Saygin, N. Bellassai, R. D'Agata, G. Spoto, F. Biscarini, *Biosensors and Bioelectronics*, 182 (2021) 113144.
22. Q. Jia, S. Huang, M. Hu, Y. Song, M. Wang, Z. Zhang, L. He, *Sensors and Actuators B: Chemical*, 323 (2020) 128647.
23. Q. Li, S. Zhou, T. Zhang, B. Zheng, H. Tang, *Biosensors and Bioelectronics*, 150 (2020) 111866.
24. H. Zhao, Q. Liu, J. Wang, A. Huang, B. Qiu, Z. Lin, *Electrochimica Acta*, 399 (2021) 139423.
25. J. Yi, W. Xiao, G. Li, P. Wu, Y. He, C. Chen, Y. He, P. Ding, T. Kai, *Applied Microbiology and Biotechnology*, 104 (2020) 9877–9890.
26. X. Dong, X. Yan, M. Li, H. Liu, J. Li, L. Wang, K. Wang, X. Lu, S. Wang, B. He, *Electrochemistry Communications*, 120 (2020) 106835.
27. K. Mao, H. Zhang, Z. Wang, H. Cao, K. Zhang, X. Li, Z. Yang, *Biosensors and Bioelectronics*, 148 (2020) 111785.
28. K. Mao, J. Ma, X. Li, Z. Yang, *Science of The Total Environment*, 688 (2019) 771–779.
29. G. Xu, J. Hou, Y. Zhao, J. Bao, M. Yang, H. Fa, Y. Yang, L. Li, D. Huo, C. Hou, *Sensors and Actuators B: Chemical*, 287 (2019) 428–436.
30. B. Wei, K. Mao, N. Liu, M. Zhang, Z. Yang, *Biosensors and Bioelectronics*, 121 (2018) 41–46.
31. M. Majdinasab, M. Daneshi, J. Louis Marty, *Talanta*, 232 (2021) 122397.
32. S.G. Liu, D. Zhang, Y. He, W. Gao, X. Shi, *Biosensors and Bioelectronics*, 166 (2020) 112461.
33. O. Alkhamis, J. Canoura, H. Yu, Y. Liu, Y. Xiao, *TrAC Trends in Analytical Chemistry*, 121 (2019) 115699.
34. H. Ren, Z. An, C.-H. Jang, *Microchemical Journal*, 146 (2019) 1064–1071.

35. S. Umrao, V. Jain, Anusha, B. Chakraborty, R. Roy, *Sensors and Actuators B: Chemical*, 267 (2018) 294–301.
36. H. Sun, N. Wang, L. Zhang, H. Meng, Z. Li, *Chemosensors*, 10 (2022) 255.
37. Y. Luan, N. Wang, C. Li, X. Guo, A. Lu, *Antibiotics*, 9 (2020) 787.
38. F. Li, Z. Yu, X. Han, R.Y. Lai, *Analytica Chimica Acta*, 1051 (2019) 1–23.
39. X. Zhao, X. Dai, S. Zhao, X. Cui, T. Gong, Z. Song, H. Meng, X. Zhang, B. Yu, *Spectrochimica Acta Part A: Molecular and Biomolecular Spectroscopy*, 247 (2021) 119038.
40. W. Xiang, Q. Lv, H. Shi, B. Xie, L. Gao, *Talanta*, 214 (2020) 120716.
41. X. Miao, W. Wang, T. Kang, J. Liu, K.-K. Shiu, C.-H. Leung, D.-L. Ma, *Biosensors and Bioelectronics*, 86 (2016) 454–458.
42. Q. Xiao, J. Li, X. Jin, Y. Liu, S. Huang, *Sensors and Actuators B: Chemical*, 297 (2019) 126740.
43. H.-A. Rafiee-Pour, M. Behpour, M. Keshavarz, *Biosensors and Bioelectronics*, 77 (2016) 202–207.
44. V.-S. Raducanu, F. Rashid, M.S. Zaher, Y. Li, J.S. Merzaban, S.M. Hamdan, *Sensors and Actuators B: Chemical*, 304 (2020) 127376.